Growth mechanism and corrosion behavior of ceramic coatings on aluminum produced by autocontrol AC pulse PEO

YongJun Guan[a,b], Yuan Xia[a,*], Guang Li[a]

[a] Institute of Mechanics, Chinese Academy of Sciences, Beijing 100190, China
[b] State Key Laboratory of Automotive Safety and Energy, Department of Automotive Engineering, Tsinghua University, Beijing 100084, China

Abstract

Ceramic coatings are produced on aluminum alloy by autocontrol AC pulse Plasma Electrolytic Oxidation (PEO) with stabilized average current. Transient signal gathering system is used to study the current, voltage, and the transient wave during the PEO process. SEM, OM, XRD and EDS are used to study the coatings evolution of morphologies, composition and structure. TEM is used to study the micro profile of the outer looser layer and inner compact layer. Polarization test is used to study the corrosion property of PEO coatings in NaCl solution. According to the test results, AC pulse PEO process can be divided into four stages with different aspects of discharge phenomena, voltage and current. The growth mechanism of AC PEO coating is characterized as anodic reaction and discharge sintering effect. PEO coating can increase the corrosion resistance of aluminum alloy by one order or two; however, too long process time is not necessarily needed to increase the corrosion resistance. In condition of this paper, PEO coating at 60 min is the most protective coating for aluminum alloy substrate.
© 2008 Elsevier B.V. All rights reserved.

1. Introduction

Plasma electrolytic oxidation (PEO) is a new technology to produce ceramic coatings on aluminum alloys [1–8], magnesium alloys [9–14], titanium alloys [15–19], aluminum matrix composite [20,21], magnesium matrix composite [22], and aluminized steel [23,24]. Besides process technology, coating's microstructure and properties, growth mechanism of PEO coating in different condition is gaining more and more attention [25–31]. In general, PEO coating on aluminum alloy contains two sublayers: inner compact layer with high hardness and outer porous layer with moderate hardness. The composition of PEO coating is mainly α-Al$_2$O$_3$ in the inner layer and γ-Al$_2$O$_3$ in the outer layer; and the composition can be adjusted easily by changing the electrolyte. Compared with traditional coatings, PEO coatings have excellent anticorrosion performance and wear resistance.

During plasma electrolytic oxidation, complex physical and chemical process occurs near the interface between electrolyte and the electrode. Due to the extreme nonlinearity of plasma discharge, monitoring the evolution of electronic signals, microstructure and corrosion behavior is helpful in understanding the mechanism underlying PEO process. Current density is one the most important parameter during PEO process. While considering growth mechanism of PEO coating, it is always ambiguous to specify the current density as growing coating will change the electrical property of the circuit.

In this paper, growth mechanism and anticorrosion behavior of ceramic coatings on aluminum alloy produced by autocontrol

* Corresponding author. Tel.: +86 10 82543858; fax: +86 10 82543858.
E-mail addresses: gyj@tsinghua.edu.cn (Y. Guan), xia@imech.ac.cn (Y. Xia).

AC pulse PEO equipment with stabilized average current system are studied. The stabilized average current system contains transient signal detector and control system. The morphology, structure, composition and corrosion behavior of PEO coatings are studied by SEM, XRD, TEM, EDS and potentiodynamic polarization test.

2. Experimental details

The details of PEO equipment and control system were shown in reference [7,27]. During the PEO process, the transient signal detector gathers the signals of current and voltage, and calculates the corresponding average values. If the gathered positive and negative currents differ from the preset ones, feedback control system will change the pulse widths to keep the currents constant. The positive pulse width and negative pulse width are controlled separately. In this paper, the ratio of positive current to negative current is set to one with a current density of 0.3 mA/mm^2. Al–Cu–1 Mg 2024 aluminum alloy plates with the size of 22 mm×l7 mm×3 mm were used as the substrate materials, and aqueous solution of sodium silicate with concentration of 20 g/L was used as the electrolyte. To study the evolution of microstructure and corrosion behavior, the process time is extended to 4 h.
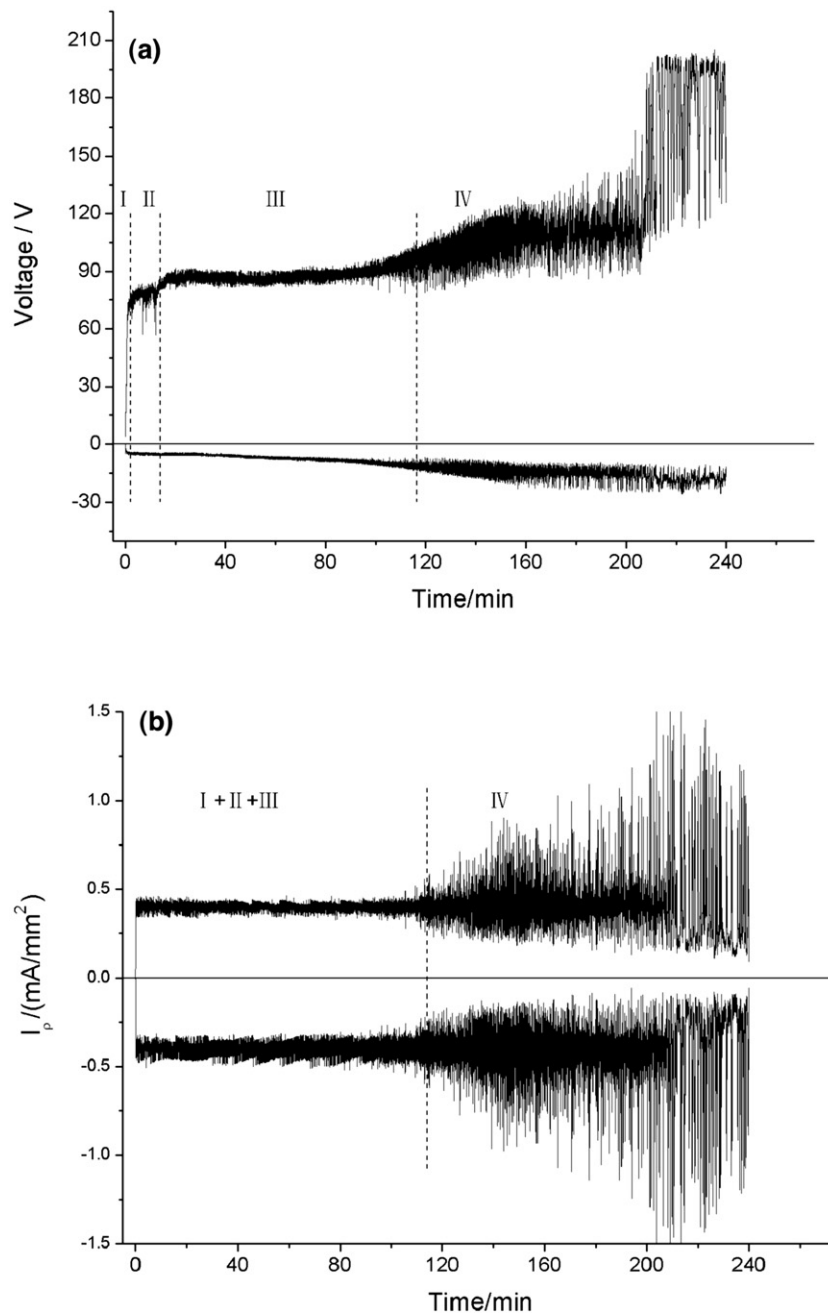

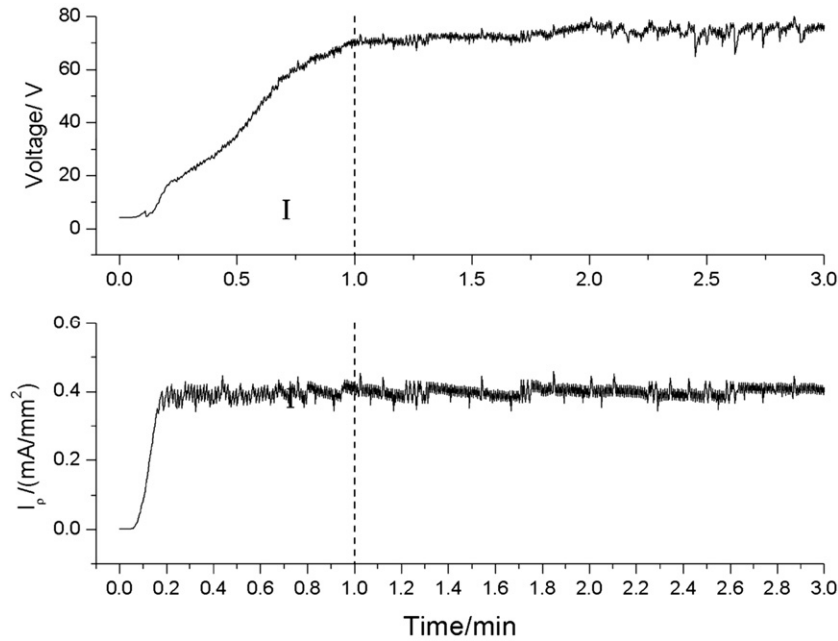Fig. 1. Evolution of voltage and current during PEO process.

Fig. 2. Evolution of voltage and current density during initial stage of PEO process.

The morphology, structure, composition of PEO coatings are studied by SEM, OM, XRD, TEM, and EDS. Potentiodynamic polarization experiments in 3.5% NaCl solution were conducted using a CHI660A electrochemistry work station with saturated calomel electrode (SCE) as the reference electrode and platinum electrode as the counter electrode. Before measurement, the working electrode was immersed in NaCl solution at open circuit potential for about 10 min until a steady state was reached. During the potentiodynamic polarization test, the scanning rate is 10 mV/s.

3. Results

3.1. Average voltage and current evolution

The evolution of current and voltage is shown in Fig. 1. According to the evolution of voltage (Fig. 1a), the PEO process can be divided into four stages. In the first stage, positive voltage increases from 0 V to 75 V in 1 min. In the second stage, the voltage stops increasing with a platform in the positive voltage curve; and this stage duration is about 12 min. In the
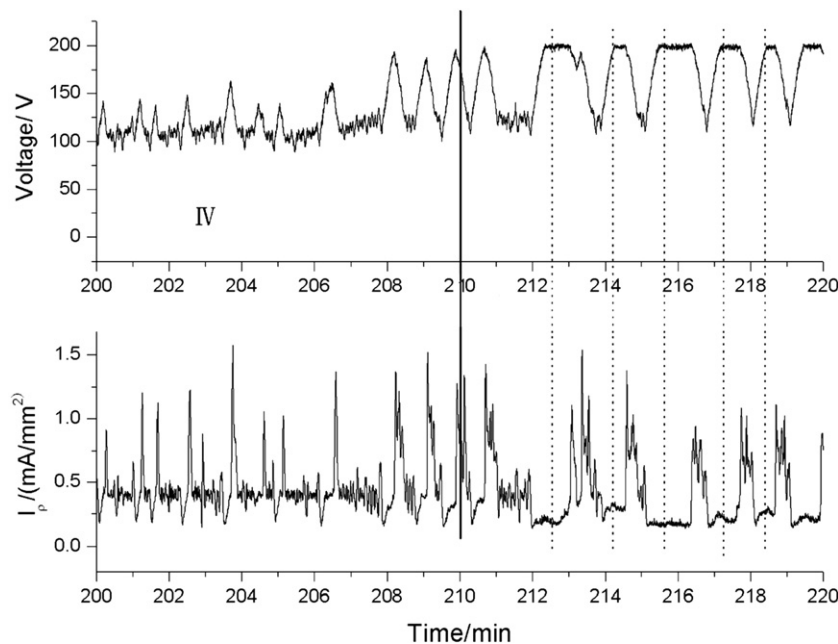

Fig. 3. Periodical fluctuation of voltage and current density during the finally stage of PEO process.

third stage, the positive voltage increases to 85 V quickly and then keeps almost constant. In the last stage, the voltage increases to the upper limit of the power supply with severe fluctuation in the voltage curves. According to the evolution of current density (Fig. 1b), the current density is kept as preset value except for the last stage. In the last stage, although the fluctuation of current density appears in the curve, the lower limit of current density decreases to zero with increasing process time.

According to the initial current density and voltage shown in Fig. 2, once the current density reaches the preset value, voltage begins to increase with a high rate which confesses the formation of passivation layer on the aluminum substrate. Fig. 3 shows the local details of current density and voltage in the last stage. Periodical fluctuation appears in both current density and voltage. Because of the current stabilization systems, the fluctuation direction of current density reverses that of voltage. During the period of voltage at upper limit with current density at lower limit, PEO coating has excellent dielectric property and plasma discharge appear in the local spot of the specimen which will destroy the coating. After the coating is destroyed by local severe discharge, the discharge disappears; and the period of voltage at lower limit and current density at upper limit comes. These processes repeat until the lower limit of current density decreases to zero when PEO process stops.
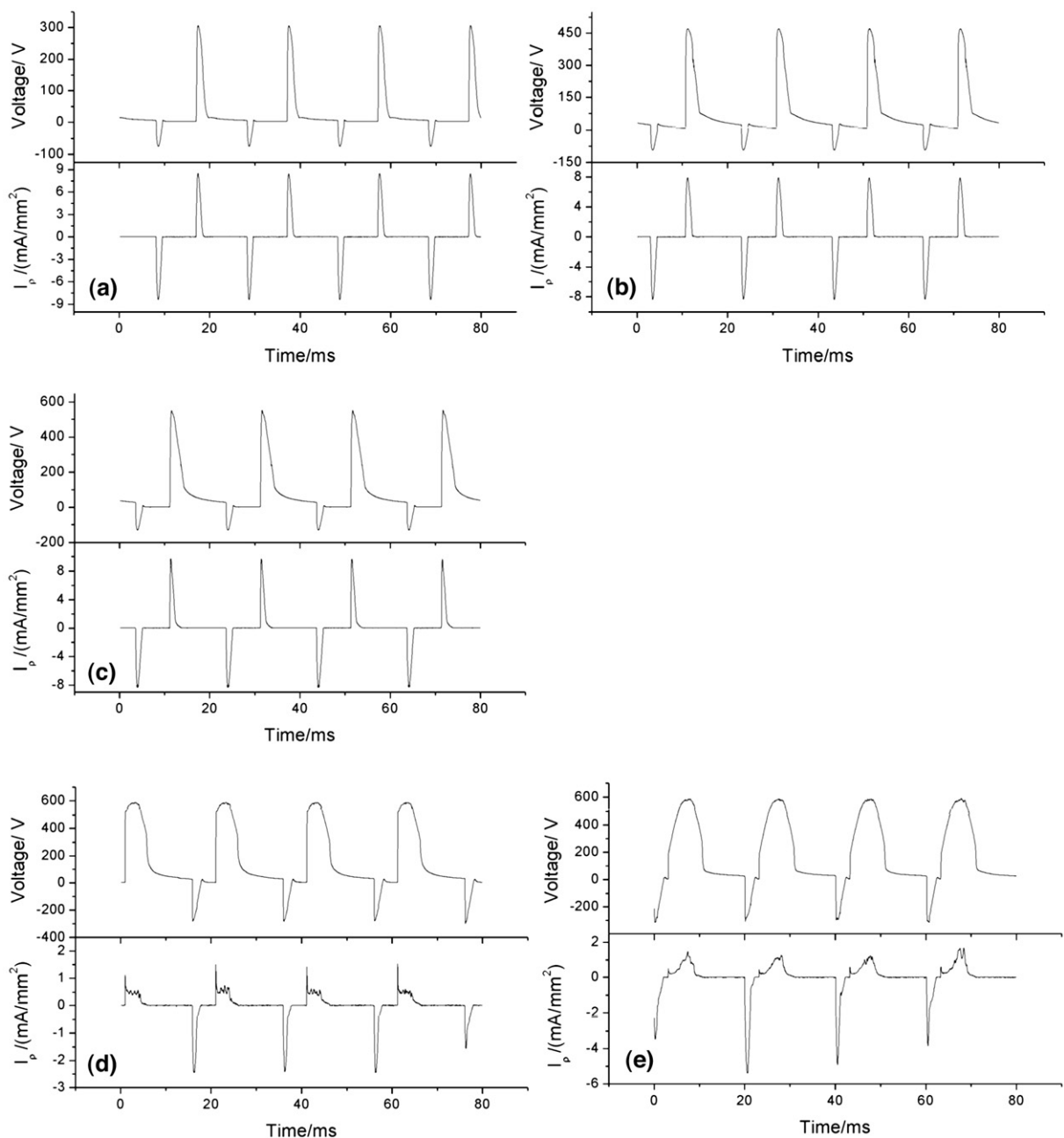

Fig. 4. Wavelet of current density and voltage during PEO process (a: the first stage; b: the second stage; c: the third stage; d, e: the fourth stage).

3.2. Instant voltage and current evolution

The wavelet of current density and voltage for the former three stages is shown in Fig. 4a, b, and c respectively, and that for the fourth stage is shown in Fig. 4d and e. According to Fig. 4, the wavelet of current density and voltage is in the same phase. The peak value of voltage increases monotonously in the former two stages, and keeps constant with increase in pulse width during the third stage. In the last stage, two kinds of wavelet appear: one is low average voltage with high average current density (Fig. 4d), and the other is high average voltage with low average current density (Fig. 4e).

Plasma discharge phenomena are different in these stages. The first stage is a discharge-free state. Continuous, tiny, white discharge appears during the second stage. The discreteness of discharge increases and the color turn to be yellow during the third stage. With the fluctuation of current and voltage in the last stage, periodical discharge state comes. The period of discharge is on the level of minute, so waveform corresponding to discharge state and non-discharge state can be determined respectively. It should be mentioned that during the last stage, discharge state corresponds to lower average current with higher average voltage (Fig. 4e), and non-discharge state corresponds to high average current with lower average voltage (Fig. 4d).

3.3. Morphology evolution

Fig. 5 shows the initial evolution of surface morphology. After 1 min of PEO process, initial wear track can be observed on the specimen surface, and sintered ceramic particle can not be observed. After 3 min of PEO process with discharge lasting for about 2 min, ceramic particles with diameter of about 1 μm appears on the surface and the initial wear track can not be observed any longer. After 7 min PEO process, the diameter of sintered ceramic particle increases to 5 μm. Surface morphologies of PEO coating for one-hour interval are shown in Fig. 6. The diameters of sintered ceramic particle are in the scope from 30 μm to 50 μm, increasing with the process time. However, after 2 h process, the change of sintered ceramic particles in size is relatively small compared with the initial morphology evolution. During the whole period of PEO process, discharge channel exits in each sintered ceramic particle.
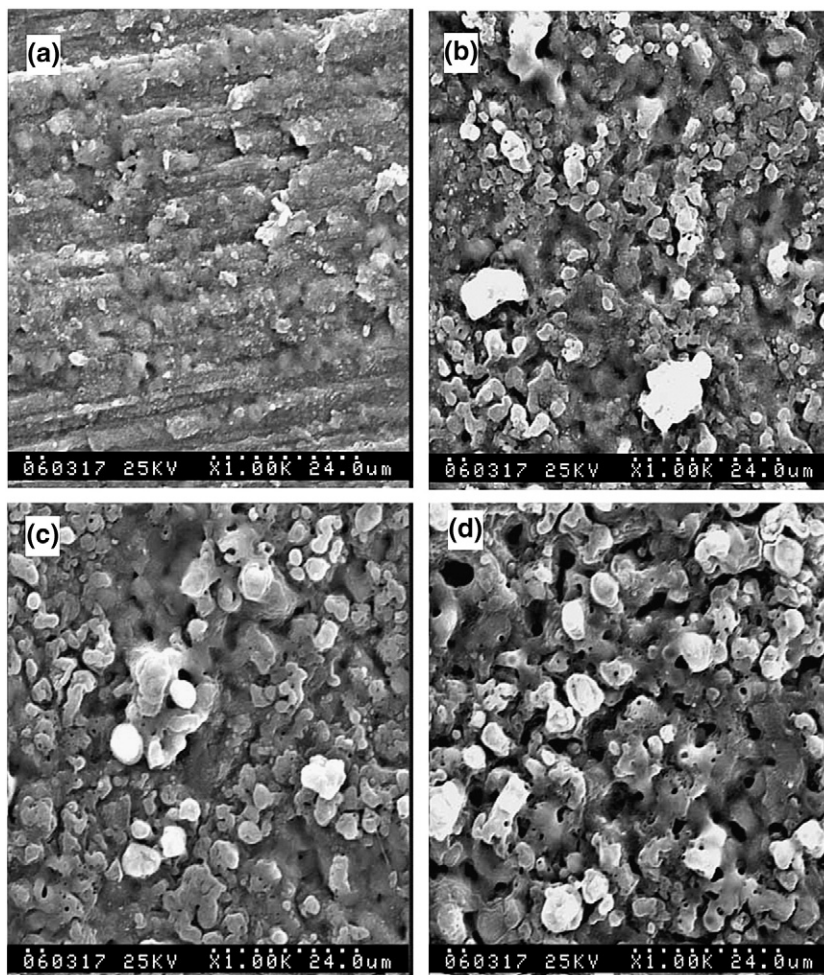

Fig. 5. Initial surface morphologies of PEO coatings (a: 1 min, b: 3 min, c: 5 min, d: 7 min).
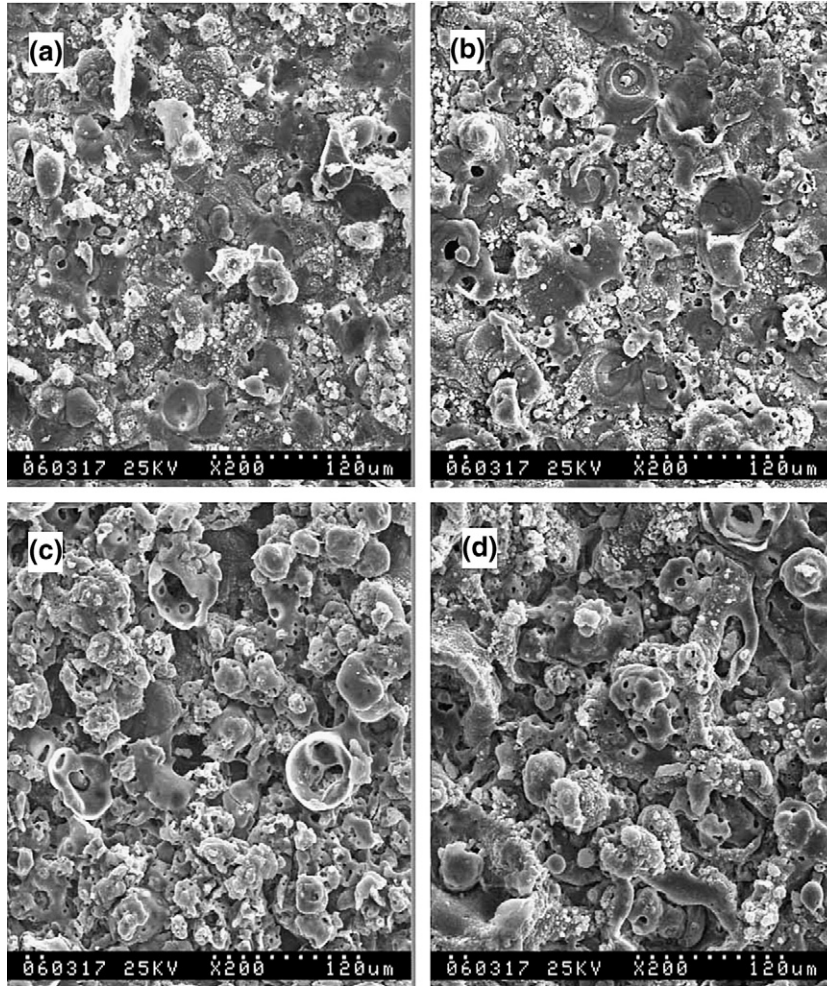
Fig. 6. Surface morphologies of PEO coatings during whole process (a: 60 min, b:120 min, c:180 min, d: 240 min).

Before plasma discharge initiates, anodic oxidation reaction occurs with a production of high dielectric passivation layer existing on the specimen surface. Voltage increases to make the anodic oxidation process continue until the critical voltage is reached and discharge phenomena appear. It can be seen from initial surface morphologies (Fig. 5) that the transition from anodic oxidation to plasma discharge oxidation is achieved in 3 min. According to the wavelet of voltage and current density (Fig. 4), the peak value of discharge energy increases quickly in the first and second stages, and then keeps almost constant in the rest stages. The size of sintered ceramic particle is determined by temperature field near the discharge channel. So the size of sintered ceramic particle changes in the same trend as discharge energy.

The cross section morphology evolution of PEO coating is shown in Fig. 7. During the whole period of PEO process, PEO
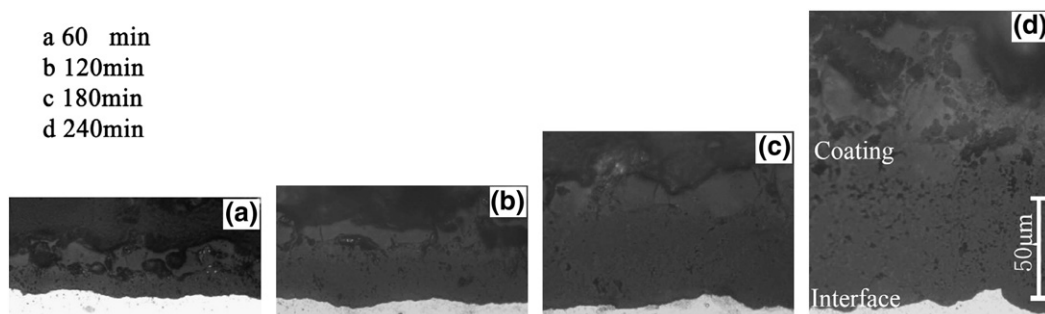

Fig. 7. Cross section morphologies of PEO coatings.

coating has a typical two-layer structure with a porous outer layer and compact inner layer. The reason for two-layer structure can be explained as different transient temperature field in outer layer and in inner layer. Because of periodical increasing and decreasing in surface temperature due to periodical plasma discharge, melt and solidification occur in the outer layer repeatedly, leading to a porous structure. The transient temperature in the inner layer is lower than that in the outer layer, phase transformation in solids occurs in the inner layer, leading to compact structure.

3.4. Composition and structure

Fig. 8 is the TEM results for PEO coating. The inner layer is composed of compact crystal particle with the size of about 500 nm; and electron diffraction proves the inner layer to be crystal structure (Fig. 8a). There are some small voids in the outer layer, with a compound structure of amorphous matter and crystal matter (Fig. 8b). Because of the high cooling rate, high temperature phase is kept in the outer layer; while the inner part of PEO coating has been transformed into compact crystal phase due to phase transformation in solids.
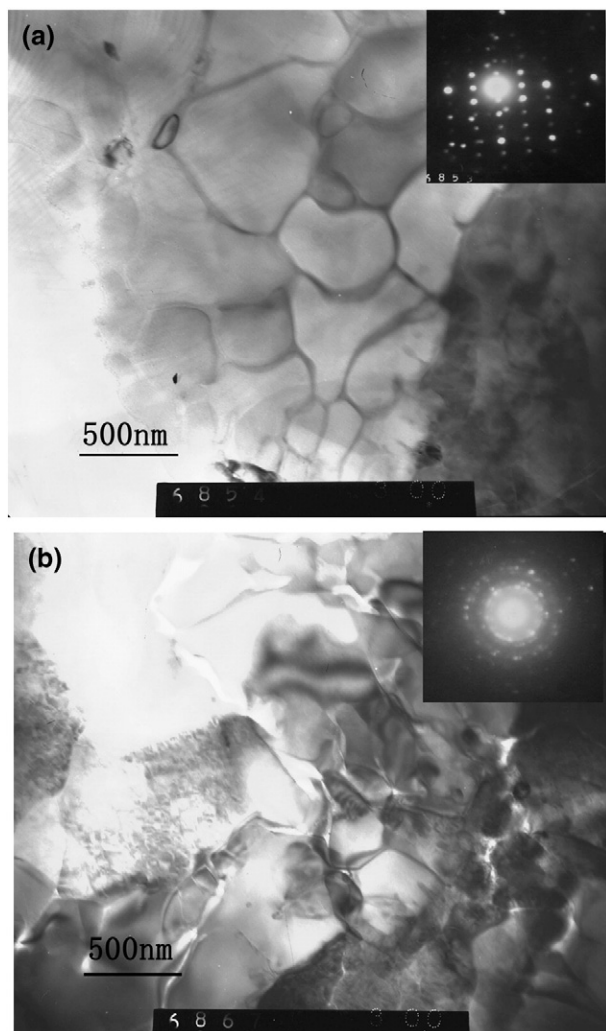

Fig. 8. TEM results of PEO coating (a: inner layer, b: outer layer).

Fig. 9 shows the XRD results of ceramic coating during PEO process. After 1 h process, γ-Al$_2$O$_3$ is the main structure companied with some mullite structure. If process time is extended to 2 h, γ-Al$_2$O$_3$, mullite, α-Al$_2$O$_3$ and δ-Al$_2$O$_3$ are the main structures in the ceramic coating. Afterward, there is no any other structure appearing in the coating. The diffraction peak of substrate Al is high in the initial time, and then decreases with process time increasing. The Al peak in XRD at 4 h is very low compared with the other component, showing the absence of Al in the ceramic coating. The melting point of alumina is 2303 K, which is near to the boiling point of Al, 2723 K, so possible Al element in the coating will be transformed in to ceramic phase with the other elements due to high temperature.

Fig. 10a and b show the EDS results for the outer layer and the inner layer respectively. The main elements in PEO coating are Al, O, Si, Cu, and Mg. O and Si in PEO coating come from electrolyte, and the other elements come from substrate alloy. Fig. 11 shows the elements distribution along the coating depth. Being constant along the coating depth, O content changes suddenly at the interface. However, Si content in outer layer is higher than that in inner layer, and the grade of Si content at the interface is lower than that of O, showing a lower diffusion coefficient of Si than that of O. Evident irregularity appears in the coating for Cu and Mg with a relatively low concentration. As there no grade in the inner layer for Al, O, and Si, it may be indicated that these three elements in PEO coating have fixed ratio, existing as compound instead of admixture. Appearance of Cu and Mg in the outer layer proves the involvement of alloy elements in the reaction process of PEO coating. Because of the different effect of alloy elements, the properties of PEO coatings differ from each other even with the same process parameters.

Fig. 12 shows the evolution of elements in PEO coating. The contents of elements for inner layer are shown in Fig. 12a, and that for outer layer are shown in Fig. 12b. Al and O are the principle elements in inner layer companied with a little Si. Si has a higher content in outer layer than that in inner layer. It can be seen that contents of O and Al is almost constant during PEO process in both outer layer and inner layer except for the last stage.

3.5. Corrosion behavior

Fig. 13 shows the polarization curves in NaCl solution for various PEO coatings. The polarization results are listed in Table 1. All of the corrosion potential of various PEO coatings increase compared with Al substrate. PEO coating at 120 min has the highest increase in corrosion potential, 0.262 mV, while PEO coating at 240 min has the lowest one, 0.143 mV. According to the test results, corrosion current density for all the coated specimens decreases by at least one order. PEO coating at 60 min has the least corrosion current density, 1.268×10^{-7} A/cm^2, which is less than that of uncoated specimen, 1.952×10^{-5} A/cm^2, by two orders. Corrosion current density increases with the increasing of process time. As the corrosion rate is proportional to the corrosion current
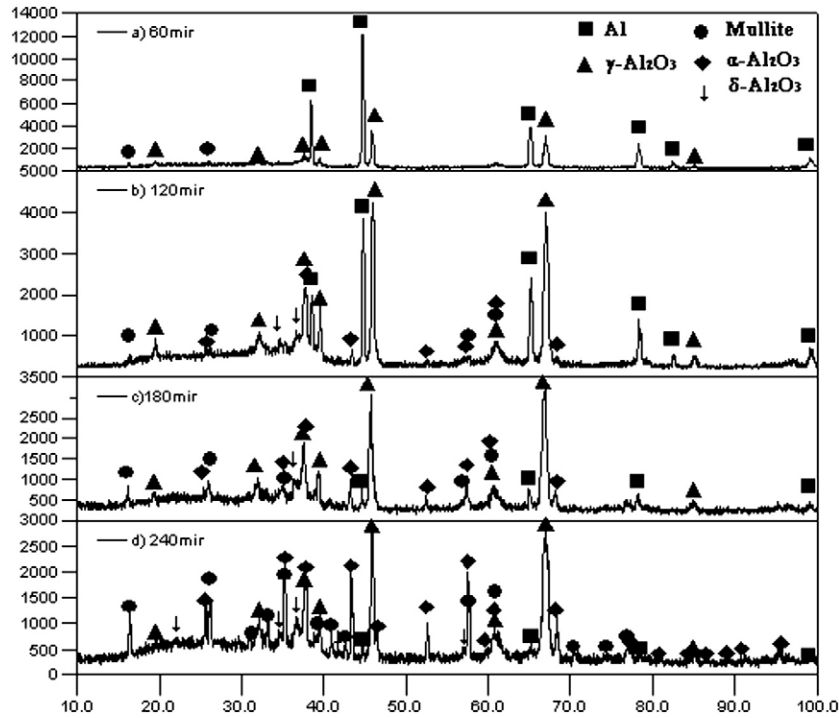
Fig. 9. XRD of PEO coatings.

density, PEO coating at 60 min is the most protective coating for Al substrate.

4. Discussion

The growth of mechanism is manifested by the increasing critical voltage and electric resistance which can be indicated by the gathering waveform of voltage and current. In the previous work, correlation between transient current-voltage property and coatings microstructure during pulse DC PEO process was studied [27]. Using the same method, transient current-voltage property evolution during pulse AC PEO can also be determined which is shown in Fig. 14. Critical voltage

and electric resistance increases rapidly in the initial stage. In fact, the initial stage of PEO process is very important to get ceramic coating with perfect interface adhesion. The interface property of PEO coating produced by autocontrol AC pulse PEO is studied in another paper [32].

5. Conclusions

Autocontrol AC pulse PEO process can be divided into four stages. The first stage is a discharge-free state. Continuous, tiny, white discharge appears during the second stage. The discreteness of discharge increases and the color turn to be yellow during the third stage. With periodical fluctuation of current and voltage in
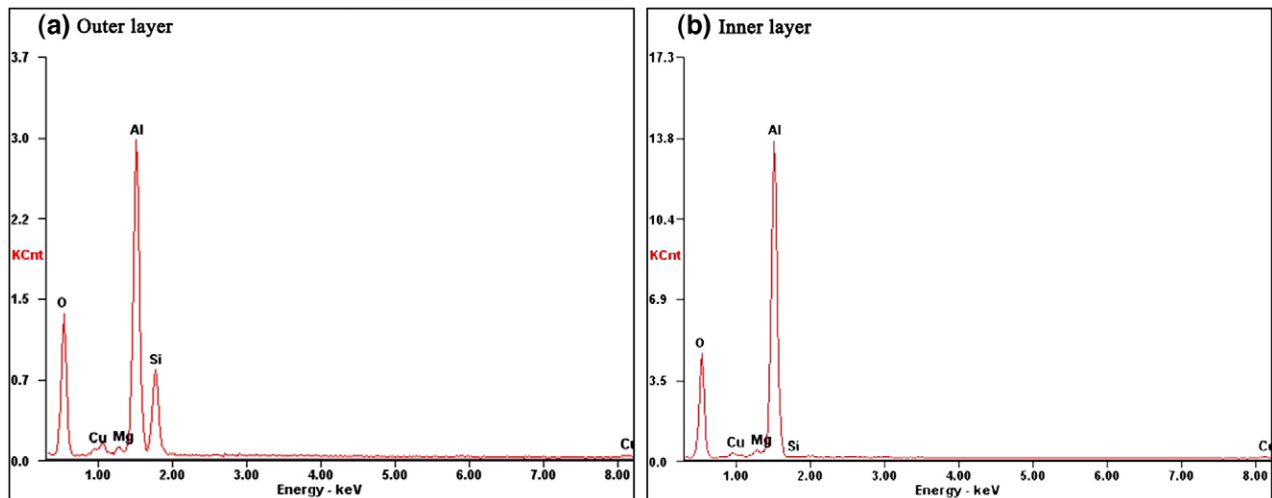

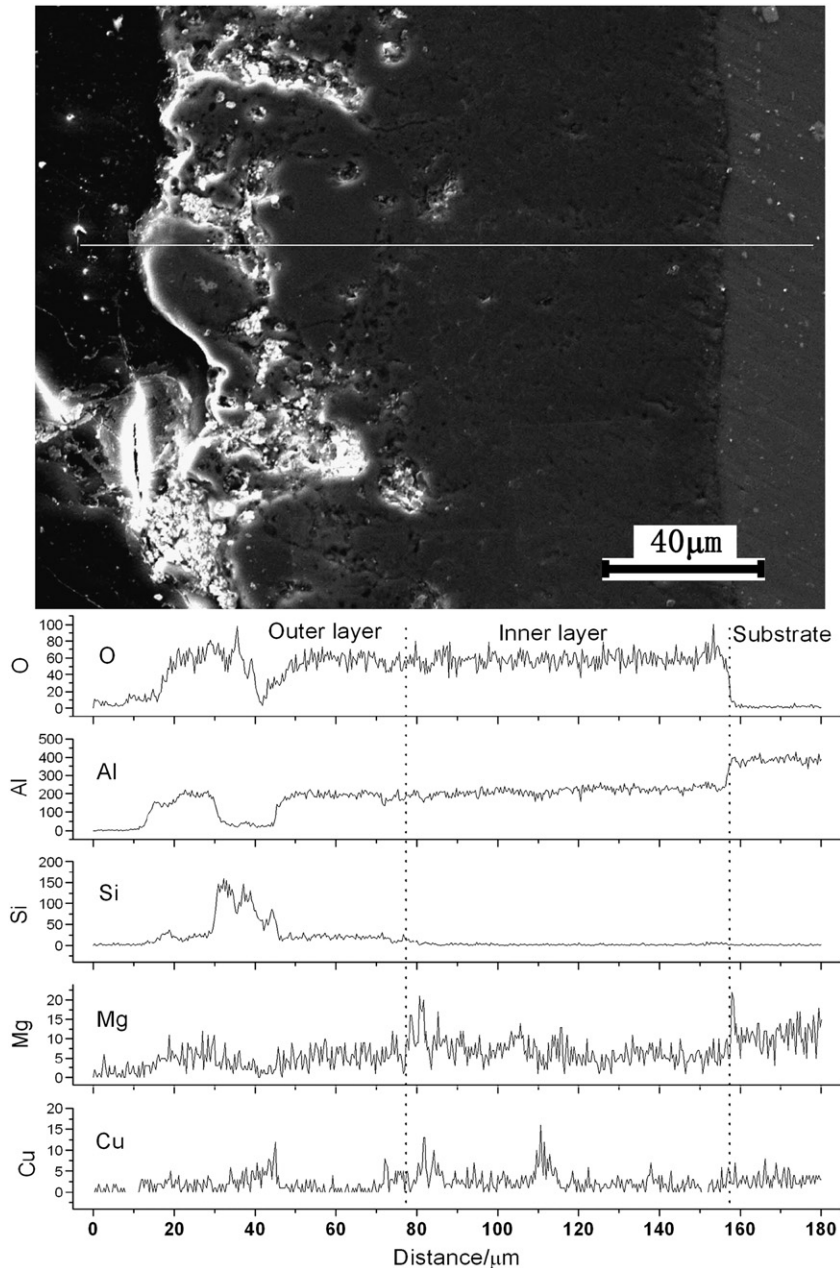Fig. 10. EDS of PEO coating (a: outer layer, b: inner layer).

Fig. 11. Elements distribution along the thickness of PEO coating.

the last stage, periodical discharge phenomena occur. In the last stage, discharge state corresponds to lower average current with higher average voltage, and non-discharge state corresponds to high average current with lower average voltage.

The size of sintered ceramic particle is determined by temperature field near the discharge channel. The peak value of discharge energy increases quickly in the first and second stages, and then keeps almost constant in the rest stages. So the size of sintered ceramic particle changes in the same trend. Repetitive melt and solidification in the outer layer leads to amorphous structure with porous morphology; transformation in solids leads to crystal structure with compact morphology.

PEO coatings can increase the corrosion resistance by one or two orders; however, increasing process time is not necessarily needed to increase the corrosion resistance. In condition of this paper, PEO coating at 60 min is the most protective coating for Al substrate.

Acknowledgement

References

[1] F. Monfort, A. Berkani, E. Matykina, P. Skeldon, G.E. Thompson, H. Habazaki, K. Shimizu, Corrosion Science 49 (2) (2007) 672.
[2] L. Wang, X. Nie, Thin Solid Films 494 (1–2) (2006) 211.

[3] D.T. Asquith, A.L. Yerokhin, J.R. Yates, A. Matthews, Thin Solid Films 515 (3) (2006) 1187.

[4] W.B. Xue, J.C. Du, X.L. Wu, Y.C. Lai, ISIJ International 46 (2) (2006) 287.

[5] S.G. Xin, L.X. Song, R.G. Zhao, X.F. Hu, Thin Solid Films 515 (1) (2006) 326.

[6] A.L. Yerokhin, A. Shatrov, V. Samsonov, P. Shashkov, A. Pilkington, A. Leyland, A. Matthews, Surface & Coatings Technology 199 (2–3) (2005) 150.

[7] Y.J. Guan, Y. Xia, Transactions of Nonferrous Metals Society of China 15 (3) (2005) 565.

[8] X. Nie, E.I. Meletis, J.C. Jiang, A. Leyland, A.L. Yerokhin, A. Matthews, Surface & Coatings Technology 149 (2–3) (2002) 245.

[9] H. Zhao, Z. Liu, L.J. Chen, J. Chen, Z. Han, Transactions of Nonferrous Metals Society of China 16 (2006) S1814.

[10] H.F. Guo, M.Z. An, Thin Solid Films 500 (1–2) (2006) 186.

[11] Q. Dong, C.Z. Chen, D.G. Wang, Q.M. Ji, Surface Engineering 22 (3) (2006) 177.

[12] A.V. Timoshenko, Y.V. Magurova, Surface & Coatings Technology 199 (2–3) (2005) 135.

[13] J. Liang, B.G. Guo, J. Tian, H.W. Liu, J.F. Zhou, W.M. Liu, T. Xu, Surface & Coatings Technology 199 (2–3) (2005) 121.

[14] A.L. Yerokhin, A. Shatrov, V. Samsonov, P. Shashkov, A. Leyland, A. Matthews, Surface & Coatings Technology 182 (1) (2004) 78.

[15] E. Matykina, A. Berkani, P. Skeldon, G.E. Thompson, Electrochimica Acta 53 (4) (2007) 1987.

[16] Y.M. Wang, B.L. Jiang, L.X. Guo, T.Q. Lei, Applied Surface Science 252 (8) (2006) 2989.

[17] F.Y. Jin, H.H. Tong, L.R. Shen, K. Wang, P.K. Chu, Materials Chemistry and Physics 100 (1) (2006) 31.

[18] A.L. Yerokhin, A. Leyland, A. Matthews, Applied Surface Science 200 (1–4) (2002) 172.

[19] S.V. Gnedenkov, P.S. Gordienko, O.A. Khrisanfova, T.M. Scorobogatova, S.L. Sinebrukhov, Journal of Materials Science 37 (11) (2002) 2263.

[20] W.B. Xue, X.L. Wu, X.J. Li, H. Tian, Journal of Alloys and Compounds 425 (1–2) (2006) 302.

[21] W.B. Xue, Acta Metallurgica Sinica 42 (4) (2006) 350.

[22] Y.Q. Wang, K. Wu, M.Y. Zheng, Surface & Coatings Technology 201 (1–2) (2006) 353.

[23] Z. Wu, Y. Xia, G. Li, F. Xu, Applied Surface Science 253 (20) (2007) 8398.

[24] W.C. Gu, G.H. Lv, H. Chen, G.L. Chen, W.R. Feng, G.L. Zhang, S.Z. Yang, Journal of Alloys and Compounds 430 (1–2) (2007) 308.

[25] P. Huang, K.W. Xu, Y. Han, Journal of Materials Science-Materials in Medicine 18 (3) (2007) 457.

[26] A.G. Rakoch, V.V. Khokhlov, V.A. Bautin, N.A. Lebedeva, Y.V. Magurova, I.V. Bardin, Protection of Metals 42 (2) (2006) 158.

[27] Y.J. Guan, Y. Xia, Transactions of Nonferrous Metals Society of China 16 (5) (2006) 1097.

[28] L.O. Snizhko, A.L. Yerokhin, A. Pilkington, N.L. Gurevina, D.O. Misnyankin, A. Leyland, A. Matthews, Electrochimica Acta 49 (13) (2004) 2085.

[29] G. Sundararajan, L.R. Krishna, Surface & Coatings Technology 167 (2–3) (2003) 269.

[30] L. Yerokhin, L.O. Snizhko, N.L. Gurevina, A. Leyland, A. Pilkington, A. Matthews, Journal of Physics. D, Applied Physics 36 (17) (2003) 2110.

[31] O.P. Terleeva, V.I. Belevantsev, A.I. Slonova, Protection of Metals 39 (1) (2003) 50–54.

[32] Y.J., Guan, Y., Xia, F.T., Xu, Surface & Coatings Technology (in press), doi:10.1016/j.surfcoat.2008.03.006.
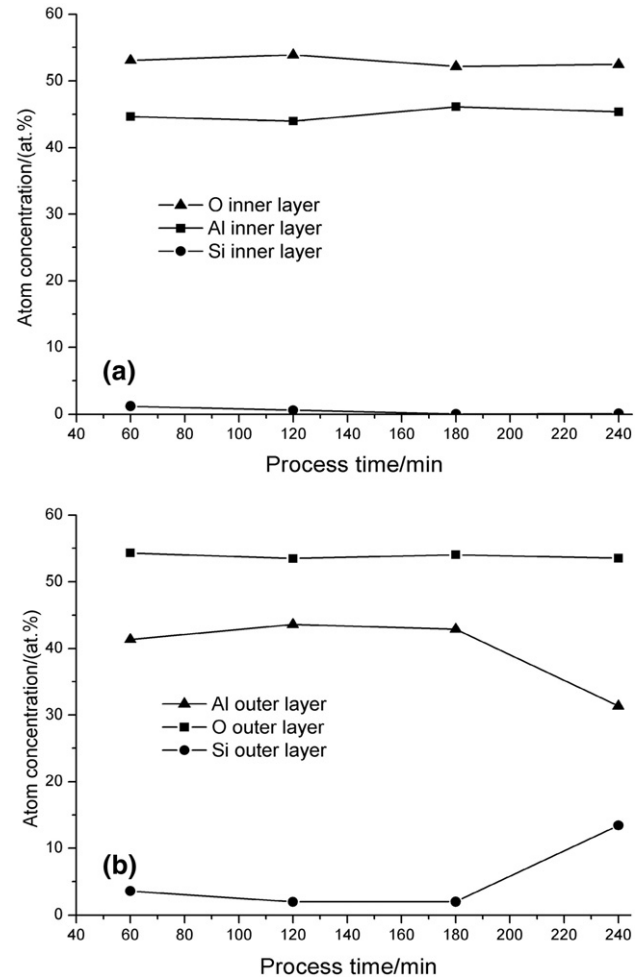
Fig. 12. Effects of process time on the content of elements in PEO coatings (a: inner layer, b: outer layer).
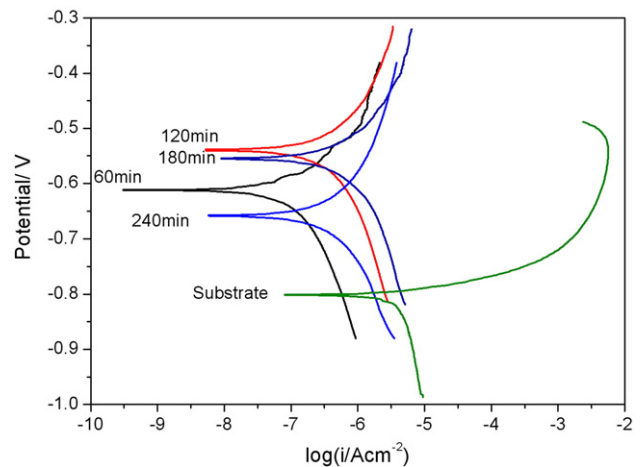

Fig. 13. Polarization curves of PEO treated samples with different process time.

Table 1
Polarization results of PEO treated samples with different process time

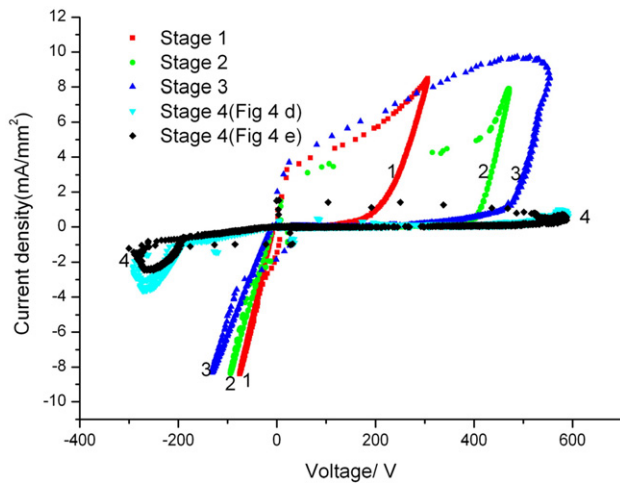| Sample	E_{corr}(V)	i_{corr}(A/cm^2)	Rp(Ω)	b_a(mV)	b_c(mV)
Substrate	−0.801	1.952×10	2.242×10^3	8.268	1.666
60 min	−0.612	1.268×10	3.083×10^5	6.991	4.131
120 min	−0.539	5.382×10	9.353×10^4	4.600	4.038
180 min	−0.555	8.598×10	5.478×10^4	5.245	3.986
240 min	−0.658	6.186×10	8.195×10^4	4.299	4.278

Fig. 14. Transient AC current–voltage property evolution during PEO process.